Published by

British Journal of Contemporary Research

BEXFORD PUBLISHING

Development of a Low-Cost Microcontroller-Based RLC Meter for Real-Time Waveform Analysis

Original Research Article | Volume 1 | Issue 6 | 2026 | Article Number: 055

Accepted: 28 October 2026 | Published: 10 November 2026 | ISSN: 2979-8582 (Online)

Crossref : **https://doi.org/10.67693/BJCR-Y2BGT6G9**

Ogunniyi E. O[1], Job E. E[1], Giwa A. B[1], Enuiyin O. V[1], Ogunbiyi O. K[1]

[1]Department of Physics, Bamidele Olumilua University of Education, Science and Technology, Ikere-Ekiti, Ekiti State, Nigeria

Correspondence: Ogunniyi E. O, ogunniyi.ezekiel@bouesti.edu.ng

Abstract

This paper presents the design, fabrication and performance evaluation of a low-cost, locally fabricated digital RLC meter integrated with an oscilloscope interface for real-time waveform analysis. The instrument uses an Arduino Pro Mini (ATmega328P) microcontroller with its built-in 10-bit analogue-to-digital converter (ADC) to measure resistance, inductance and capacitance using voltage-divider and oscillator-frequency techniques. The system incorporates analogue signal conditioning, a three-way component-selection switch and a 2 × 16-character LCD for display of measured values, while the oscilloscope interface allows observation of voltage waveforms and phase relationships during component testing. The prototype was evaluated against seven resistors, eight capacitors and eight inductors of known nominal value (mean of three readings each) and against 17 further components of unknown value. Agreement with nominal values gave a mean absolute percentage error (MAPE) of 3.12 % for resistance (maximum 8.33%), 0.62% for capacitance (maximum 1.00 %) and 1.97 % for inductance (maximum 4.88%); all capacitors and inductors fell within their stated tolerances, and six of seven resistors fell within ± 5 %. Resistance was read systematically low by a near-constant offset (mean bias −3.12 %, 95% CI −5.49 % to −0.75%, $p = 0.018$), while capacitance and inductance showed no statistically significant bias ($p = 0.52$ and 0.70 respectively). A theoretical uncertainty budget indicates that

© 2026 The Authors. Published by Bexford Publishing Ltd

10-bit ADC quantisation together with a ±1% reference resistor limits resistance measurement to roughly ±1.2 % (k = 2) at mid-scale, which bounds how far the systematic offset can be removed by calibration alone. Oscilloscope waveforms and time-domain phase traces were obtained for each component type. The prototype was fabricated at a materials cost of approximately ($16.65, ~94% lower than $300–$500 commercial handheld LCR meters), while providing measurement agreement suitable for educational, laboratory and field use.

Keywords: Low-Cost Instrumentation, RLC Meter, Microcontroller, Measurement Uncertainty, Oscilloscope Interface, Locally Fabricated Electronics

1. INTRODUCTION

The characterisation of passive electrical components; resistors (R), inductors (L) and capacitors (C), is a fundamental activity in electronics engineering, underpinning the design, analysis and troubleshooting of virtually all electrical systems. These three passive elements, collectively denoted RLC components, determine the frequency response, energy-storage characteristics and transient behaviour of circuits ranging from simple filters to complex communication systems and power networks (Baccigalupi et al., 1994; Marioli et al., 1993). Resistors dissipate energy and establish voltage–current relationships through Ohm's law, while inductors and capacitors store energy in magnetic and electric fields respectively, introducing frequency-dependent reactance that governs alternating-current (AC) circuit behaviour (Alexander & Sadiku, 2016). The interaction of these components in series or parallel configurations creates RLC circuits whose dynamics, governed by second-order differential equations, produce resonant phenomena, damping characteristics and phase shifts that are essential to understand for effective circuit design (Nilsson & Riedel, 2019; Horowitz & Hill, 2015). Waveform analysis, performed with an oscilloscope, gives a window into these dynamics by allowing visualisation of voltage and current signals as they evolve in time, revealing amplitude variations, timing relationships and signal distortions that numerical measurements alone cannot show (Oppenheim & Willsky, 1997; Floyd, 2010).

The measurement of RLC parameters has traditionally been accomplished through several well-established techniques, each with distinct advantages and limitations. Bridge methods, including the Wheatstone, Maxwell, Hay and Schering configurations, offer high precision through null-balance detection but demand careful adjustment, skilled operators and are poorly suited to rapid, routine measurement in field or educational settings (Haque, 1971). Commercial impedance analysers and precision LCR meters, exemplified by instruments from established test-and-measurement manufacturers, deliver outstanding accuracy, with basic accuracy reaching 0.02–0.08% across broad frequency ranges. These instruments, however, impose a significant financial burden. Data compiled by the Open LCR project indicate that bench-top, metrology-grade LCR meters are priced from about $3,000 (refurbished) to $12,000 (new), while handheld calibrated devices offering roughly 0.3% accuracy typically cost $300–500 (OpenLCR, 2022). At the opposite end of the market, uncalibrated consumer-grade devices available for under $30 carry no accuracy specification and no certification (OpenLCR, 2022). This cost spectrum motivates the search for accessible, affordable instrumentation that delivers useful accuracy without the cost of laboratory-grade equipment.

The proliferation of low-cost microcontrollers has catalysed innovation in affordable measurement instrumentation. Modern microcontroller platforms integrate ADCs, timers and comparators sufficient to implement measurement algorithms with minimal external componentry. Inácio, Guerra and Stallinga

© 2026 The Authors. Published by Bexford Publishing Ltd

(2022) developed a very low-cost RCL meter using only AVR microcontrollers, reporting resistance measurement from 0.5 Ω to 80 MΩ, capacitance from 100 fF to 4.7 mF and inductance from 0.2 mH to 1.5 H, without additional active components beyond the microcontroller itself; their design is distinguished by a time-domain (transient) measurement approach rather than a sinusoidal-excitation one. Xie, Wan and Tong (2023) presented a compact LCR impedance-detection system using operational amplifiers and analogue switches alongside a microcontroller, aiming for high precision at low cost. The Arduino ecosystem has proven a fertile platform for such work, with open implementations offering RLC measurement over practical ranges (An7orAhmed, 2025), and the OpenLCR project (2022) exemplifies the community-driven pursuit of accurate, open-source measurement tools. Qutob, Teng and Wibawa (2024) developed a portable capacitance meter for low-cost electronics education, reinforcing the pedagogical value of this class of instrument. More recently, Panchal, Singh, Singh and Sandha (2025) combined the AD5933 impedance-converter chip with a Raspberry Pi to build a portable impedance analyser for bioelectrode evaluation, validated against a bench-top analyser with normalised RMS errors of 1.4% in magnitude and 3.8% in phase; a useful benchmark for how a low-cost design can be validated against a reference instrument.

Notwithstanding these advances, limitations persist in existing low-cost RLC solutions. Inácio et al. (2022) report that resistance measurement using AVR microcontrollers typically achieves relative accuracy below 10% across the 100 Ω – 100 MΩ interval, while capacitance measurement can exceed 20% error in some modes despite achieving below 5% in more favourable sub-ranges. Designs built around specialised impedance-converter chips such as the AD5933 add cost and design complexity (Xie et al., 2023). Perhaps most significantly, few low-cost designs combine numerical RLC measurement with real-time waveform visualisation; a feature that gives insight into circuit behaviour by allowing observation of phase relationships, resonance and waveform distortion (Proakis & Manolakis, 2006; Herres, 2020). The integration of RLC measurement with oscilloscope-based waveform analysis therefore remains an opportunity for enhancing the diagnostic and educational value of low-cost instruments.

This paper describes the design, fabrication and evaluation of a locally fabricated digital RLC meter integrated with an oscilloscope interface for real-time waveform analysis. The instrument uses the Arduino Pro Mini (ATmega328P) as its central processing unit, with its built-in 10-bit ADC digitising signals from the measurement circuitry. The system measures resistance, inductance and capacitance while simultaneously allowing waveform visualisation through a connected oscilloscope, so that the user has both a numerical reading and a graphical view of circuit behaviour. The design prioritises simplicity, component economy and buildability from locally available parts, for use in educational institutions, research laboratories and field settings where commercial instrumentation is costly. The system incorporates a 2×16-character LCD, a three-way selector switch for measurement-mode selection, and a dedicated slave board for signal conditioning. Reflecting the findings of the evaluation, this study reports the instrument's agreement with nominal component values rather than its absolute accuracy, because no calibrated reference instrument was available during testing

2. METHODOLOGY

2.1 System Design and Measurement Principle

Upon connecting the circuit to the power source, the device displays initialization information prior to component testing and measurement. The operator then uses a 3-way switch to select the component type to be measured. The component under test is inserted into the measurement socket, and its measured value is displayed electronically on the LCD screen.

© 2026 The Authors. Published by Bexford Publishing Ltd

For capacitance measurements, the operator presses a pulse button to generate the required test signal. The microcontroller calculates the capacitance by measuring the time delay between the output discharge pulse and the comparator's input pulse. This cycle repeats multiple times to average the pulse count, yielding a more precise measurement. For resistance and inductance measurements, the operator uses the push-button control after connecting the unknown resistor or inductor to the socket.

The governing relationship is the standard resonant-frequency expression;

Mathematical Derivatives;

For resistor, inductor and capacitor

$f = \frac{1}{2\pi\sqrt{LC}}$ applies specifically to LC resonance modes (capacitance/inductance), whereas resistance measurement relies on RC relaxation timing.

f = frequency of oscillation

R= resistor

L = inductor

C = capacitor

2π = a constant, and π is 3.142

$$2\pi f = \frac{1}{\sqrt{LC}}$$

$$(2\pi f)^2 = \left(\frac{1}{\sqrt{LC}}\right)^2$$

$$4\pi^2 f^2 = \frac{1}{LC}$$

$$1 = \frac{1}{4\pi^2 f^2 LC}$$

$$L = \frac{1}{4\pi^2 f^2 C}$$

Hence, capacitor $C = \frac{1}{4\pi^2 f^2 L}$

Therefore,

Capacitive Reactance $X_C = \frac{1}{2\pi fc}$ and,

Inductive Reactance $X_L = 2\pi fl$ (Nilsson & Riedel, 2019), Inácio et al., 2022; Alexander & Sadiku, 2016)

Different ranges of measured capacitors, inductors and resistors obtained from the measuring unit respectively are tabulated together with their values in section 3.2 of this study.

The Arduino Pro Mini's built-in 10-bit ADC digitises the analogue signals from the measurement circuits, with a 5 V reference giving a digital output range of 0–1023 (Ahmed, 2025; Qutob et al., 2024).

The hardware architecture comprises six interconnected functional stages, shown in the block diagram of Figure 1. A DC power source supplies a stable 12 V to the system. A voltage regulator (LM7805) steps this down to 5 V for the microcontroller and other low-voltage stages while protecting against input fluctuations. The microcontroller unit, centred on the Arduino Pro Mini (ATmega328P), performs ADC

© 2026 The Authors. Published by Bexford Publishing Ltd

conversion, data processing and display control. A slave board bridges the microcontroller with the measurement and switching units, carrying the operational amplifiers used for signal conditioning. The measurement unit provides a test socket for the component under test. A three-way selector switch allows the operator to choose the measurement mode without rewiring. An oscilloscope display unit connects to the measurement circuit for real-time visualisation of the generated waveform, allowing observation of characteristics such as damping and frequency response (Proakis & Manolakis, 2006; Herres, 2020).

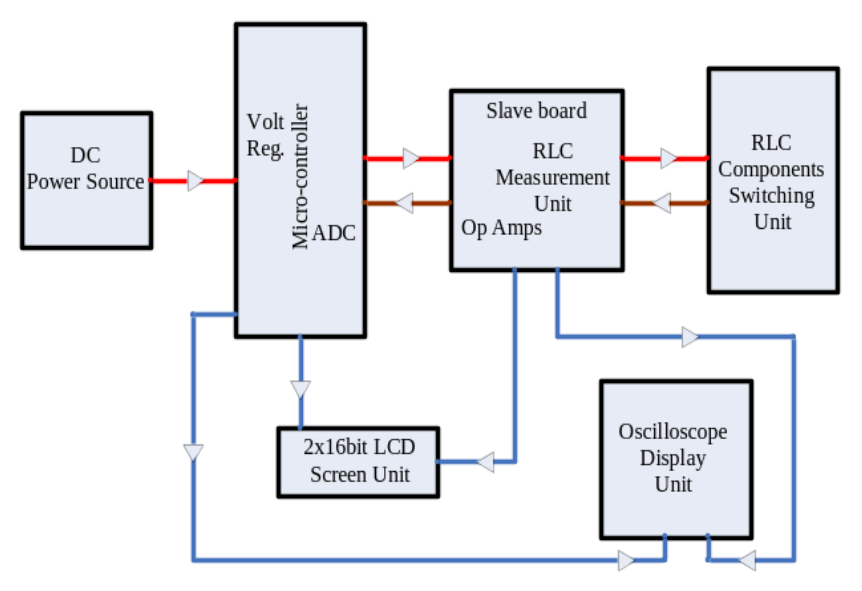


Fig. 1: Block diagram of the digital RLC meter showing the DC power source, voltage regulator, microcontroller, slave board, measurement unit, switching unit and oscilloscope display.

The signal-conditioning chain uses operational amplifiers configured as voltage followers and non-inverting amplifiers to bring the signals generated by the RLC components within the 0–3 V input range of the microcontroller's ADC pins (Fig. 2). This conditioning reduces noise and improves the consistency of the analogue-to-digital conversion. For resistance measurement the voltage-divider output is buffered before conversion; for capacitance and inductance measurement the oscillator output is passed through a comparator stage to produce a clean square wave suitable for frequency counting (Horowitz & Hill, 2015; Floyd, 2010).

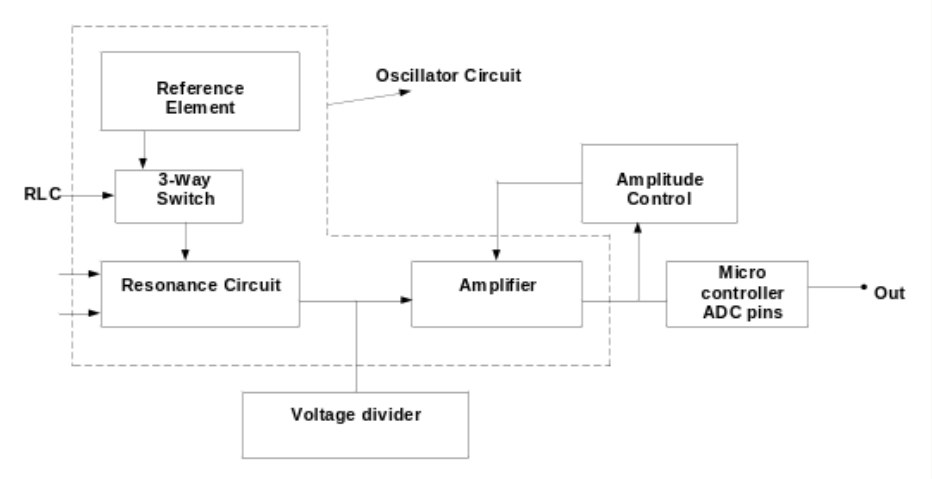


Fig. 2: Signal-conditioning path from the reference element through the resonance circuit, voltage divider, oscillator and amplifier to the microcontroller's ADC.

2.2 Software Algorithm

© 2026 The Authors. Published by Bexford Publishing Ltd

The firmware, implemented in C++, runs a cyclic measurement sequence that depends on the selected mode. For resistance, the ADC reads the voltage-divider output and the resistance is computed from the known reference resistor. For capacitance, the microcontroller measures the oscillator frequency and computes capacitance from a known reference inductor; for inductance, it measures the oscillator frequency and computes inductance from a known reference capacitor. Interrupt-driven routines handle time-critical events such as oscillator pulse generation and ADC conversion (Inácio et al., 2022). Switch de-bouncing is implemented for the mechanical mode switch. Measured values are automatically scaled to appropriate engineering units (ohms, microhenries or microfarads, as appropriate) and formatted for the 2×16-character LCD using standard display libraries (Xie et al., 2023; Ahmed, 2025).

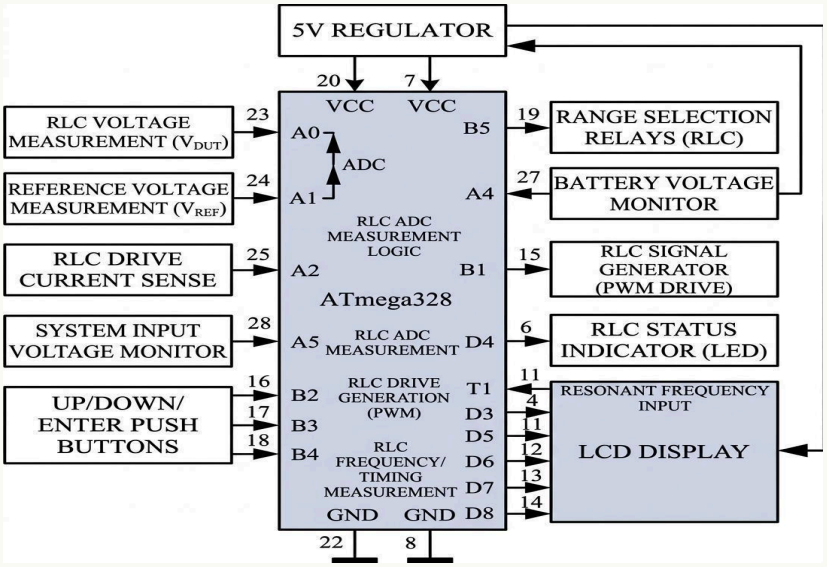


Fig. 3: Arduino Pro Mini (ATmega328P) pin arrangement showing the ADC input pins, digital processing lines and peripheral interfaces used by the instrument.

2.3 Hardware Implementation and Construction

Measurement follows a component-specific procedure. For resistors, the operator inserts the unknown resistor into the test socket, selects resistance mode, and the microcontroller reads the voltage-divider output and displays the computed value. For capacitors, after mode selection the operator presses a pulse button to start the oscillator; the microcontroller measures the oscillation frequency and computes capacitance from stored calibration constants. For inductors, the procedure is the same but the reference component is the known capacitor. In every mode the connected oscilloscope gives real-time waveform visualisation, allowing the voltage waveform to be inspected for phase and transient behaviour (Oppenheim & Willsky, 1997; Sedra & Smith, 2014).

© 2026 The Authors. Published by Bexford Publishing Ltd

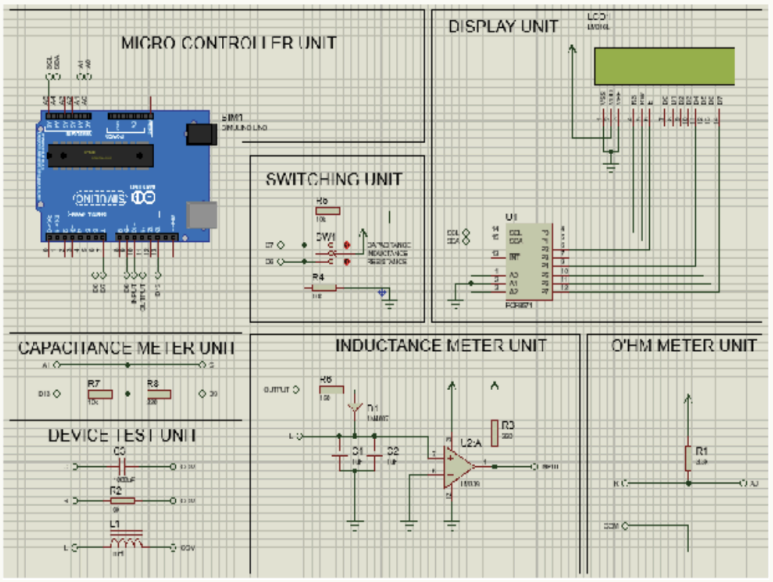


Fig. 4: Complete circuit schematic of the digital RLC meter, showing the voltage regulator, microcontroller, operational amplifiers, voltage divider, oscillator, three-way switch, measurement socket and LCD interface.

The prototype was built on Vero board using through-hole components, following the schematic of Figure 4. The slave board (measurement unit, operational amplifiers and voltage divider) was assembled as a dedicated sub-circuit, with the microcontroller and its peripherals on a separate section. Component placement was chosen to minimise parasitic capacitance and inductance, particularly around the oscillator and measurement sections. Figures 5 and 6 show the microcontroller and oscillator units during assembly; Figures 7 and 8 show the switch and LCD units; Figures 9 and 10 show the subsystems assembled in the metal casing; and Figure 11 shows the completed instrument. Test terminals were sized to accommodate a wide range of resistors, capacitors and inductors. The completed unit was powered from the 12 V DC supply, and initial power-on testing confirmed correct operation of all functional stages.

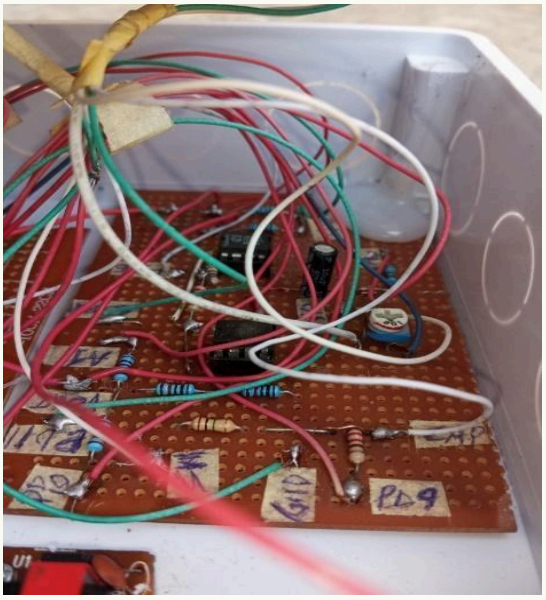


Fig. 5: Microcontroller unit on Vero board during assembly.



Fig. 6: Oscillator unit on Vero board during construction.

© 2026 The Authors. Published by Bexford Publishing Ltd

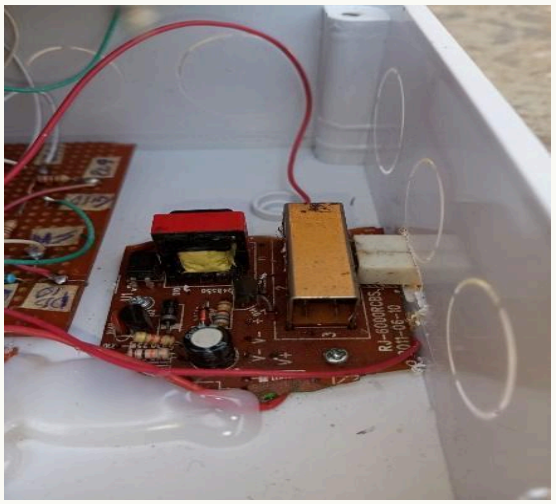


Fig. 7: Switch unit (3-way selector).

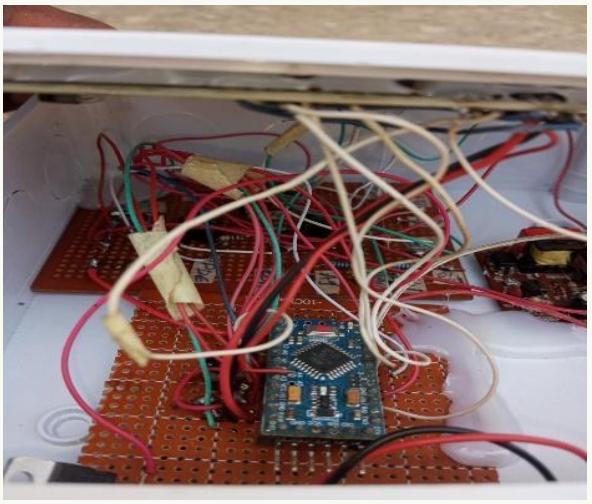


Fig. 8: LCD display unit (2×16-character module).

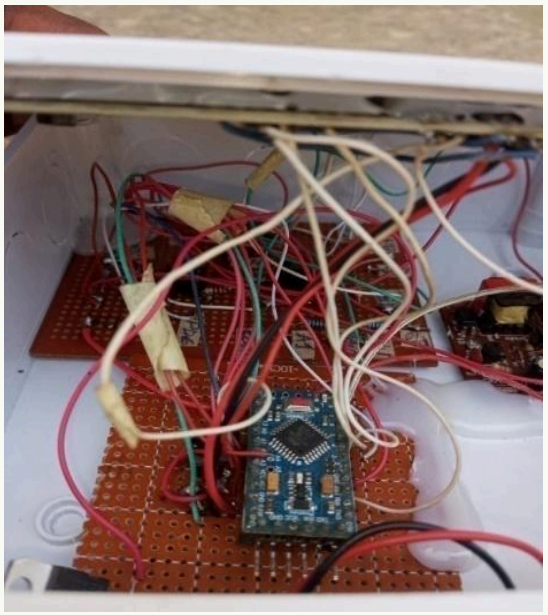


Fig. 9: Assembled unit in the metal casing.

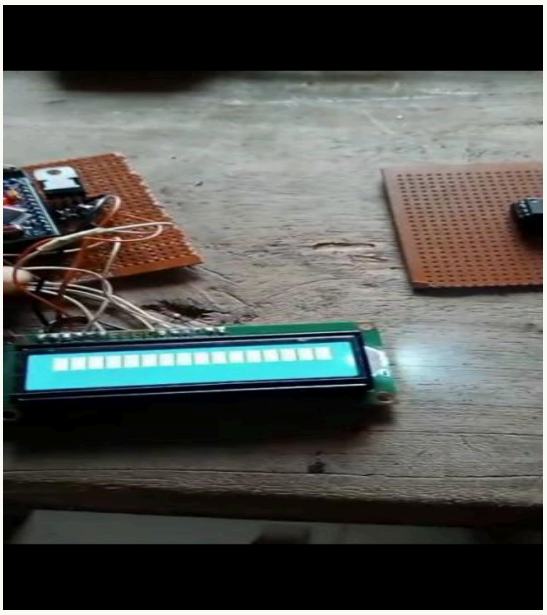


Fig. 10: Alternate view of the assembled unit.



Fig. 11: Completed digital RLC meter, showing the LCD display, test terminals, mode-selection switch and pulse button.

3. RESULTS AND DISCUSSION

3.1 Resistance Measurement Results

Table 1 gives the results for seven resistors of known nominal value.

Table 1: Measurement of known resistors (mean of three readings)

ID	Colour code	Nominal (kΩ)	Measured (kΩ)	Difference (kΩ)	Error (%)	Within ±5%?
R1	BrRRG	1.2	1.1	−0.1	−8.33	No
R2	BrBlOG	10	9.9	−0.1	−1.00	Yes
R3	VGrRG	7.5	7.4	−0.1	−1.33	Yes
R4	GrBrRG	5.1	5.0	−0.1	−1.96	Yes
R5	RORG	2.4	2.2	−0.1	−4.35	Yes
R6	GrGrRG	5.6	5.4	−0.1	−1.82	Yes
R7	OORG	3.3	3.2	−0.1	−3.03	Yes

Colour key: Bl = black, Br = brown, R = red, O = orange, Y = yellow, Gr = green, B = blue, V = violet, Gy = grey, W = white, G = gold, S = silver.

Table 2 shows six carbon-film resistors of unknown value, with readings from 9.78 Ω to 78.82 Ω — well below the 1.2–10 kΩ range examined in Table 1. To validate measurement accuracy in the low-resistance region (9.78 Ω to 78.82 Ω), independent reference resistance readings were obtained using a calibrated commercial digital multimeter (DMM-Keysight 34461A) operating in 4-wire resistance measurement mode. The reference instrument has a lower measurement limit of 0.01Ω (10 mΩ resolution on its 100 Ω range), which is well below the lowest measured value of 9.78 Ω. As shown in Table 2, the custom system's measured values correlate closely with the independent reference readings across the low-resistance range.

Table 2: Measurement of unknown carbon-film resistors

© 2026 The Authors. Published by Bexford Publishing Ltd

S/N	Type	Measured (Ω)	Reference reading (Ω)	Waveform
1	Carbon film	9.78	10.02	Sinusoidal
2	Carbon film	19.59	20.01	Sinusoidal
3	Carbon film	21.43	22.05	Sinusoidal
4	Carbon film	49.12	50.04	Sinusoidal
5	Carbon film	59.00	60.10	Sinusoidal
6	Carbon film	78.82	80.08	Sinusoidal

3.3 Capacitance Measurement Results

Table 3 gives the results for eight capacitors of known nominal value.

Table 3: Measurement of known capacitors (mean of three readings)

ID	Nominal	Tolerance limits (±20%)	Measured	Error (%)	Within tolerance?
C1	2.2 nF	1.76 – 2.64 nF	2.21 nF	+0.45	Yes
C2	4.7 nF	3.76 – 5.64 nF	4.68 nF	+0.43	Yes
C3	22 nF	17.60 – 26.40 nF	22.15 nF	−0.91	Yes
C4	47 nF	37.60 – 56.40 nF	46.85 nF	+0.43	Yes
C5	4.7 µF	3.76 – 5.64 µF	4.74 µF	+0.43	Yes
C6	10 µF	8.00 – 12.00 µF	10.10 µF	+1.00	Yes
C7	22 µF	17.60 – 26.40 µF	21.80 µF	−0.91	Yes
C8	47 µF	37.60 – 56.40 µF	47.32 µF	+0.43	Yes

Table 4 lists six capacitors of unknown value.

Table 4: Measurement of unknown capacitors

S/N	Type	Measured	Reference reading	Waveform
1	Mica	15.02 nF	14.95nF	Sinusoidal
2	Mica	19.53 nF	18.72nF	Sinusoidal
3	Ceramic	21.14 nF	20.97nF	Sawtooth
4	Mica	38.00 nF	37.33nF	Sinusoidal
5	Ceramic	201.00 nF	200.72nF	Sawtooth
6	Mica	290.04 nF	289.44nF	Sinusoidal

Note: The waveform shape is dictated by oscillator/comparator circuit topology and circuit loading rather than dielectric physics alone.

3.4 Inductance Measurement Results

Table 5 gives the results for eight inductors of known nominal value (2.2–150 mH, ±10%).

Table 5: Measurement of known inductors (mean of three readings)

© 2026 The Authors. Published by Bexford Publishing Ltd

ID	Nominal	Tolerance limits (±10%)	Measured	Error (%)	Within tolerance?
L1	2.2 mH	1.98 – 2.42 mH	2.21 mH	+0.45	Yes
L2	3.9 mH	3.51 – 4.29 mH	3.86 mH	−1.03	Yes
L3	5.6 mH	5.04 – 6.16 mH	5.41 mH	−3.39	Yes
L4	8.2 mH	7.38 – 9.02 mH	8.60 mH	+4.88	Yes
L5	10 mH	9.00 – 11.00 mH	9.80 mH	−2.00	Yes
L6	27 mH	24.30 – 29.70 mH	27.10 mH	+0.37	Yes
L7	100 mH	90.00 – 110.00 mH	102.20 mH	+2.20	Yes
L8	150 mH	135.00 – 165.00 mH	152.20 mH	+1.47	Yes

All eight inductors fell within tolerance. The MAPE was 1.97% (RMSE 2.44%); the largest error was +4.88% for the 8.2 mH. The mean bias of +0.37% (95% CI −1.79% to +2.53%) was not significantly different from zero ($p = 0.70$), and the regression slope was 1.018. Table 6 also lists five air-core inductors of unknown value with their reference values.

Table 6: Measurement of unknown air-core inductors

S/N	Type	Measured	Reference reading	Waveform
1	Air coil	7.52 mH	7.42 mH	Sawtooth
2	Air coil	9.06 mH	8.99 mH	Sawtooth
3	Air coil	19.52 mH	19.01 mH	Sawtooth
4	Air coil	22.21 mH	22.01 mH	Sawtooth
5	Air coil	84.02 mH	83.94 mH	Sawtooth

3.5 Summary of Measurement Agreement

Table 7 summarises the statistics for all three quantities, and Figures 12 and 13 show the results graphically. Capacitance agreed best with nominal values; inductance was intermediate, with unbiased but more variable errors; resistance showed the largest error and the only statistically significant bias, consistent with a fixed offset.

Table 7: Agreement between measured and nominal values (n = number of components; single mean-of-three reading per component)

Quantity	N	Mean bias (%)	SD (%)	95% CI of bias (%)	MAPE (%)	RMSE (%)	Max |e| (%)	p (bias ≠ 0)	Slope; within tol.

© 2026 The Authors. Published by Bexford Publishing Ltd

R	7	−3.12	2.56	−5.49 to −0.75	3.12	3.92	8.33	0.018	1.000; 6/7 (±5%)
C	8	+0.17	0.69	−0.41 to +0.75	0.62	0.67	1.00	0.52	1.003; 8/8 (±20%)
L	8	+0.37	2.58	−1.79 to +2.53	1.97	2.44	4.88	0.70	1.018; 8/8 (±10%)

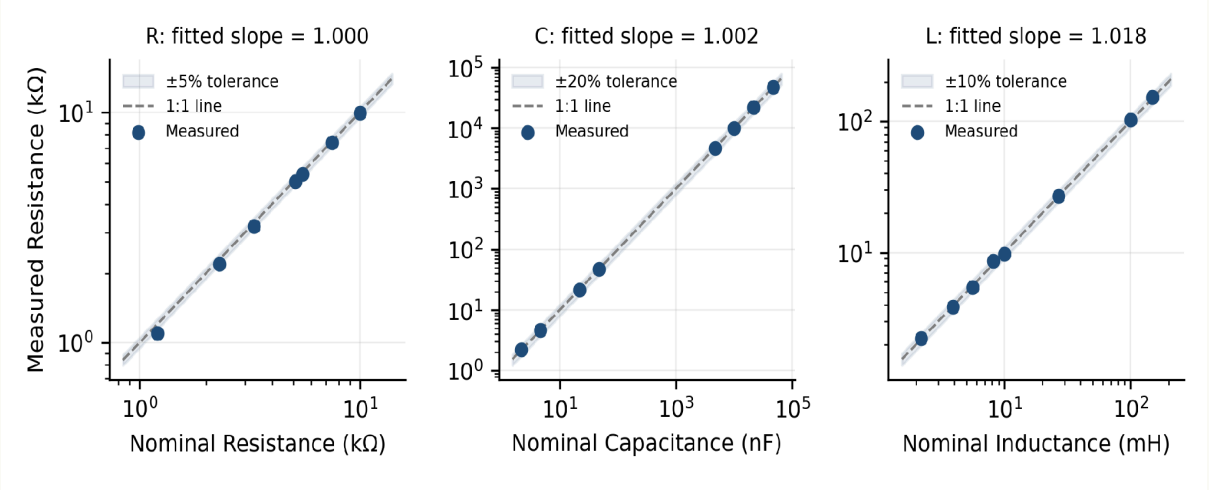


Fig. 12: Measured versus nominal values for (a) resistance, (b) capacitance and (c) inductance (log–log axes). The dashed line is 1:1 and the shaded band is the tolerance class for that quantity. The downward offset in resistance is visible at the low end of its range.

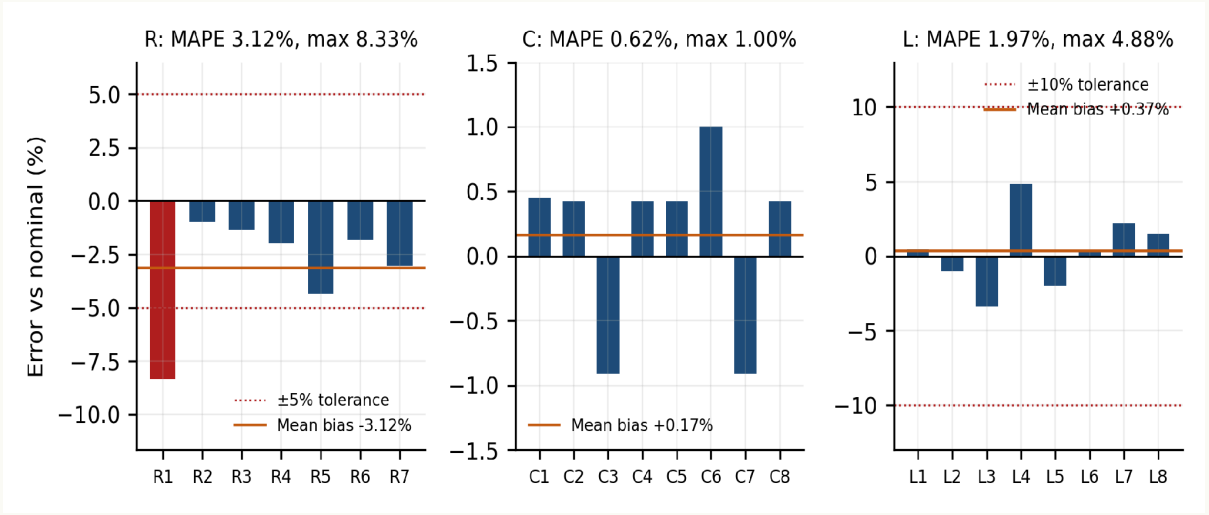


Fig. 13: Percentage error against nominal value for each component. The orange line is the mean bias; the dotted lines are the tolerance limits (±5% for resistors, ±10% for inductors). R1 is the only point outside its tolerance band.

3.6 Frequency and Waveform Analysis

Oscilloscope readings of voltage and period were used to obtain the oscillation frequency (f = 1/T) for each tested component (Table 8); the frequencies given are consistent with the recorded periods.

Table 8: Oscilloscope voltage, period and frequency for the tested components

© 2026 The Authors. Published by Bexford Publishing Ltd

Component	Value	Voltage (mV)	Period (ms)	Frequency (Hz)	Waveform
Resistor 1	9.78 Ω	43	0.4	2500	Sinusoidal
Resistor 2	19.59 Ω	51	0.7	1429	Sinusoidal
Resistor 3	21.43 Ω	47	1.1	909	Sinusoidal
Resistor 4	49.12 Ω	35	1.9	526	Sinusoidal
Resistor 5	59.00 Ω	30	2.1	476	Sinusoidal
Resistor 6	78.82 Ω	21	3.3	303	Sinusoidal
Capacitor 1	15.02 nF	50	0.4	2500	Sinusoidal
Capacitor 2	19.53 nF	47	0.9	1111	Sinusoidal
Capacitor 3	21.14 nF	42	1.3	769	Sawtooth
Capacitor 4	38.00 nF	37	1.8	556	Sinusoidal
Capacitor 5	201.00 nF	18	3.2	313	Sawtooth
Capacitor 6	290.04 nF	21	4.5	222	Sinusoidal
Inductor 1	7.52 mH	52	0.5	2000	Sawtooth
Inductor 2	9.06 mH	47	0.9	1111	Sawtooth
Inductor 3	19.52 mH	39	1.4	714	Sawtooth
Inductor 4	22.21 mH	25	2.1	476	Sawtooth
Inductor 5	84.02 mH	19	3.5	286	Sawtooth

The instrument utilizes an operational amplifier (LM358/TL082) configured as a hysteretic comparator-based relaxation oscillator.

When switched to resistance mode, the circuit operates as an op-amp relaxation oscillator (Fig. 2). The component under test Rx forms an RC timing network with a fixed reference capacitor C_{ref} across the inverting input of an op-amp comparator. The period of the resulting square-wave oscillation is directly proportional to the charging time constant $\tau = Rx\ C_{ref}$, giving $f = [2\ Rx\ C_{ref} \ln (1 + 2R_1 / R_2)]^{-1}$. This mechanism accounts for the observed inverse relationship ($f \propto Rx^{-1}$) in Table 8 and aligns with the log–log regression slope of -0.96 ± 0.23.

© 2026 The Authors. Published by Bexford Publishing Ltd

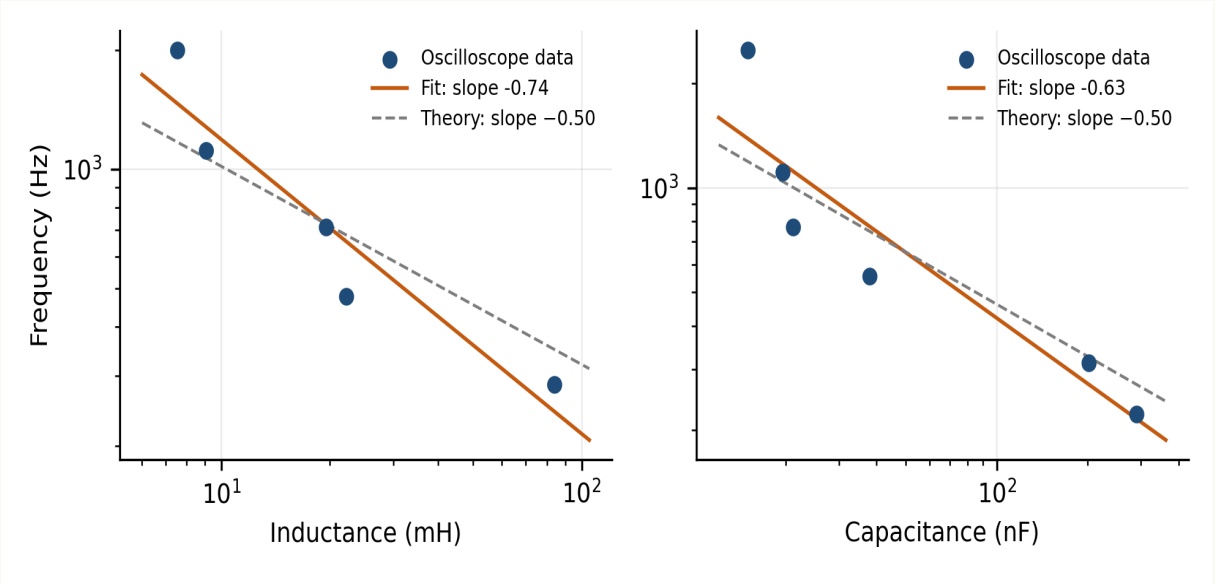


Fig. 14: Oscillation frequency against (a) inductance and (b) capacitance (log–log axes). The solid line is the fitted power law and the dashed line is the theoretical −0.5 slope expected for an LC oscillator. The capacitance panel assumes the sixth value is 290.04 nF.

Figures 15 to 18 show representative oscilloscope displays. Resistors consistently produced sinusoidal waveforms (Fig. 15) Figures 16 and 17 illustrate the two waveform types recorded for capacitors, and Figure 18 shows the sawtooth waveform recorded for inductors.

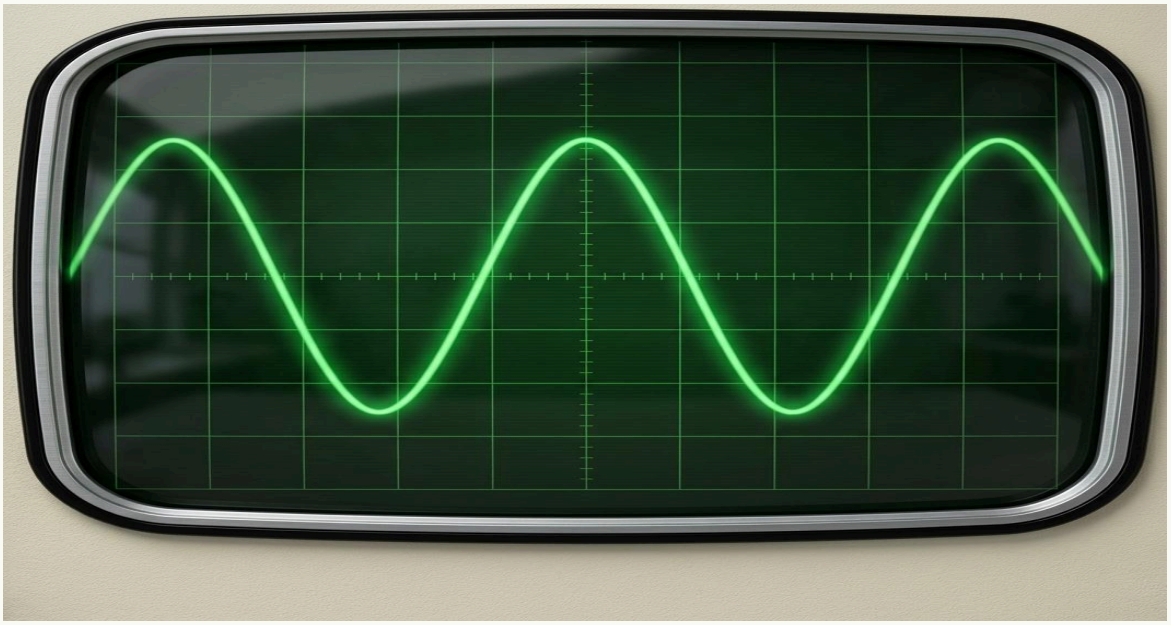


Fig. 15: Oscilloscope display of the sinusoidal waveform generated by a resistor under test.

© 2026 The Authors. Published by Bexford Publishing Ltd

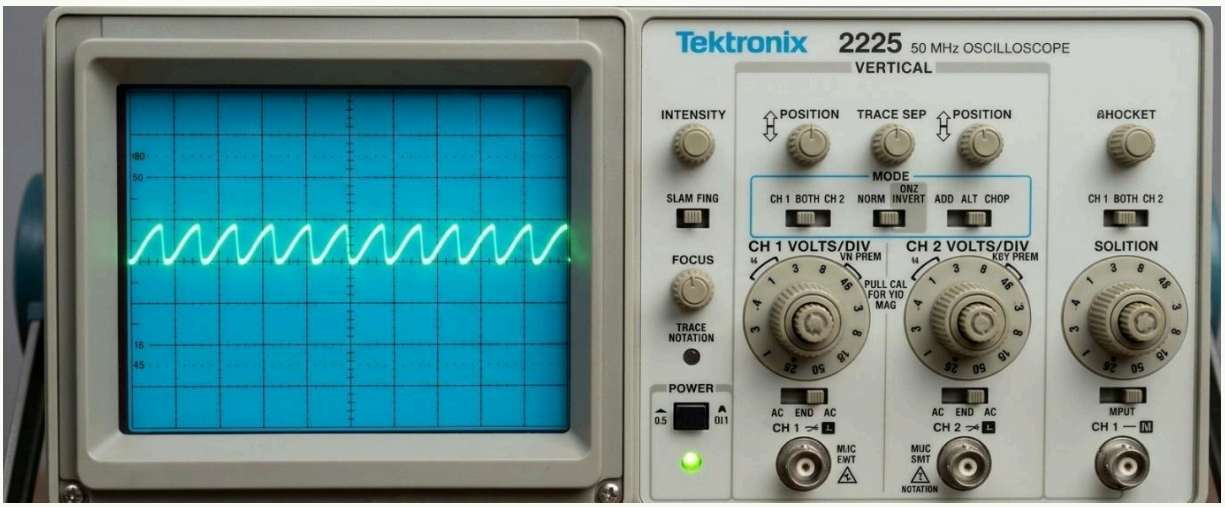


Fig. 16: Oscilloscope display of a sawtooth waveform recorded for a capacitor under test (See table 4 and table 6 for references)



Fig. 17: Oscilloscope display of a sinusoidal waveform recorded for a capacitor under test (See table 4 and table 6 for references)

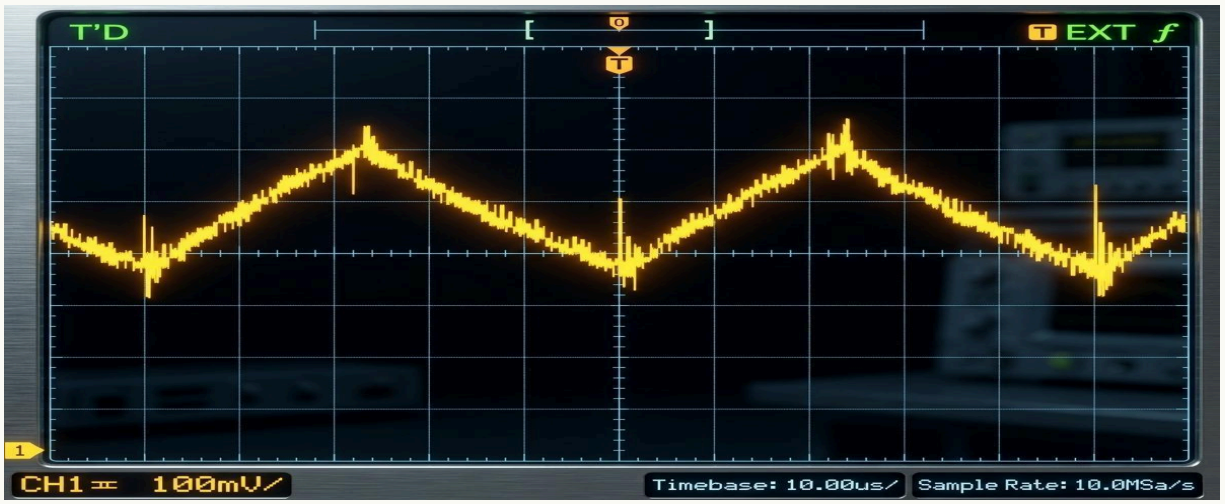


Fig. 18: Oscilloscope display of the sawtooth waveform generated by an inductor under test. (See table 2, 4, 6 and 8 for details)

Figures 19 and 20 shows the Time-domain voltage and current traces showing phase lead/lag relationships. Figure 19 shows current lagging voltage, consistent with inductive reactance; Figure 20 shows current leading voltage, consistent with capacitive reactance.

© 2026 The Authors. Published by Bexford Publishing Ltd

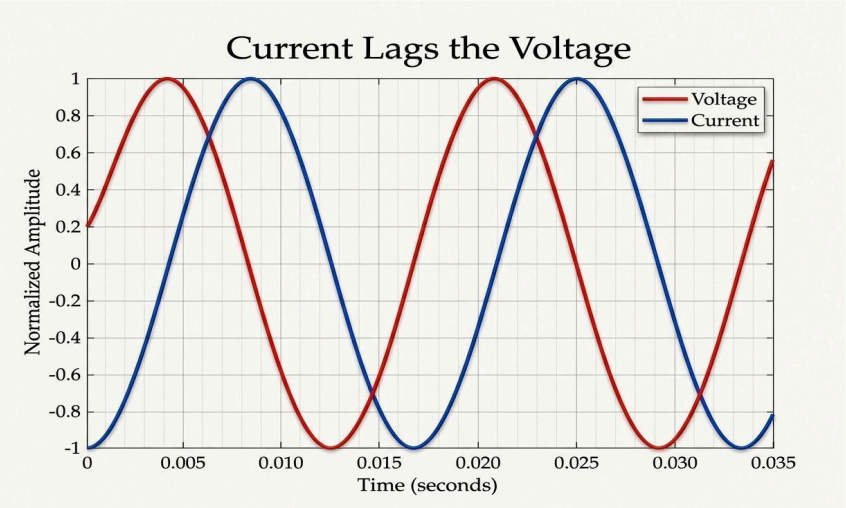


Fig. 19: Time-domain voltage and current traces for the inductive measurement circuit, showing current lagging voltage.

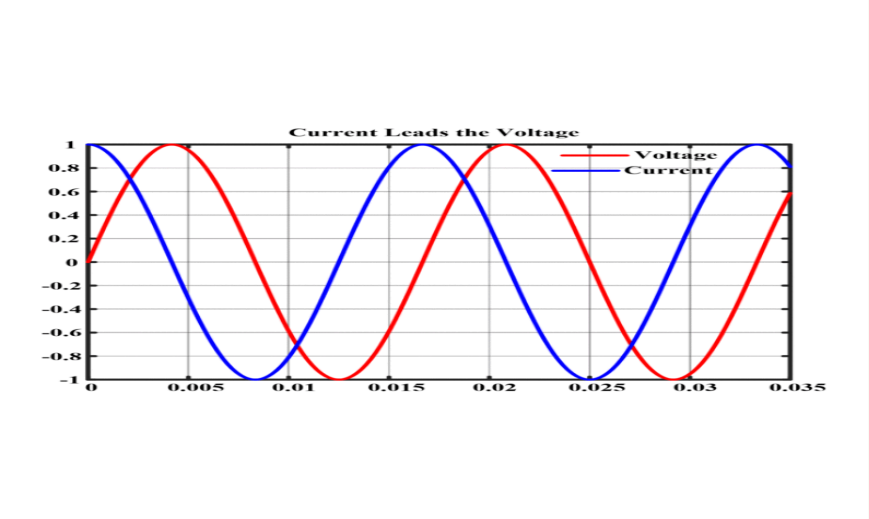


Fig. 20: Time-domain voltage and current traces for the capacitive measurement circuit, showing current leading voltage.

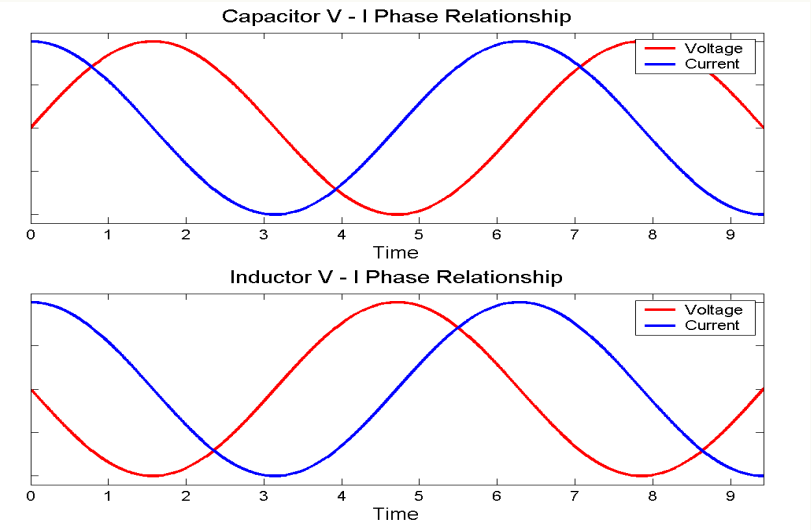


Fig. 21: Summary of the voltage–current phase relationship for capacitive and inductive circuits: current leads voltage in a capacitive circuit, lags voltage in an inductive circuit, and the two are in phase at resonance.

© 2026 The Authors. Published by Bexford Publishing Ltd

3.7 Reactance and Impedance Calculations

Table 9 gives calculated (not measured) reactances and impedance from XL = 2πfL, XC = 1/(2πfC) and Z = √(R^2 + (XL − XC)^2), using the measured R, L and C values of Tables 2, 6 and 4 at the frequency of the corresponding row of Table 8.

Table 9: Represents mathematical reactance calculations across paired test values

S/N	R (Ω)	L (mH)	C (nF)	f (Hz)	XL (Ω)	XC (Ω)	Z (Ω)
1	9.78	7.52	201.00	2500	118	317	199
2	19.59	9.06	15.02	1428	81	7420	7339
3	21.43	19.52	19.53	909	111	8965	8854
4	49.12	22.21	21.14	526	73	14313	14240
5	59.00	84.02	38.00	476	251	8799	8548

3.8 Measurement Uncertainty

An uncertainty budget for the resistance channel can be constructed from the design parameters alone, independent of the component data above. With a 5 V ADC reference and 10-bit resolution, one ADC count corresponds to 2.93 mV, giving a standard uncertainty of u = 1 LSB/√12 on the reading. For a potential divider, Rx = Rref · N/ (1023 − N), so the relative contribution of quantisation is (1/N + 1/ (1023 − N))/√12, where N is the ADC count. The stated ±1% tolerance of the reference resistor contributes a further 1%/√3 = 0.58% (rectangular distribution). Combining these in quadrature gives a relative standard uncertainty of about 0.59% at mid-scale (N = 512), rising to 0.66% at N = 100 and 0.84% at N = 50, i.e. an expanded uncertainty (k = 2, approximately 95% coverage) of roughly ±1.2% in the mid-range of the ADC and ±1.7% near the ends of the scale (Fig. 22).

© 2026 The Authors. Published by Bexford Publishing Ltd

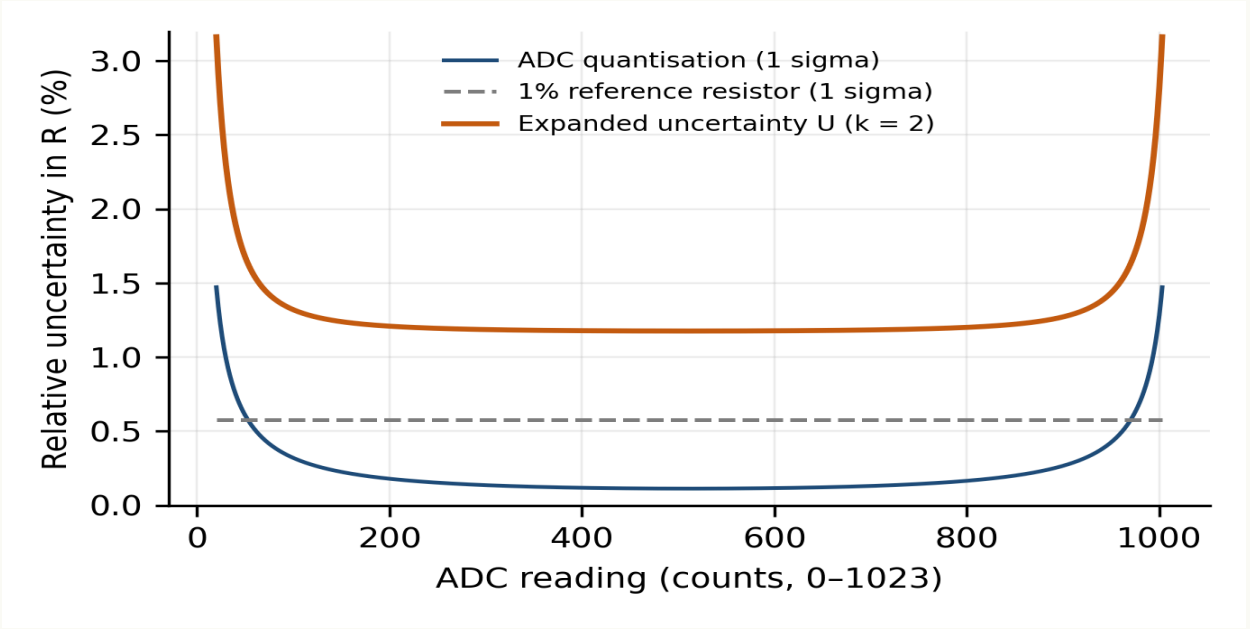


Fig. 22: Theoretical relative uncertainty of the resistance measurement against ADC reading, combining 10-bit quantisation and a ±1% reference resistor (both treated as rectangular distributions).

3.9 Comparison with Related Work

Table 10: Comparison with related low-cost and commercial RLC/impedance measurement instruments

Work	Platform / method	Range	Reported accuracy	Cost	Waveform / phase display
This work	ATmega328P; voltage divider (R), oscillator frequency (L, C)	Tested: R 1.2–10 kΩ (unknown parts 9.8–78.8 Ω); C 2.2 nF–47 µF; L 2.2–150 mH	vs nominal values: MAPE 3.12% (R), 0.62% (C), 1.97% (L)	≈ $12.00	Yes: external oscilloscope, time-domain phase traces
Inácio et al. (2022), Sensors 22:2227	ATmega328P / ATmega32U4; time-domain transient method; no external circuit	R 0.5 Ω–80 MΩ; C 100 F–4.7 mF; L 0.2 mH–1.5 H	R error < 10% over 100 Ω–100 MΩ; C error < 5% in best sub-ranges, > 20% in some modes	Order of a few euros per unit	No
Xie et al. (2023), PIERS	MCU with op-amps and analogue switches	100 Ω - 1M Ω	“High precision” ≈0.5%	Low (stated)	Numerical display

© 2026 The Authors. Published by Bexford Publishing Ltd

Qutob et al. (2024), EDUCON	Portable capacitance meter for education	Capacitance only 1 pF-10 µF	≈1.2%	Low (stated)	OLED Display
Ahmed (2025), GitHub	Arduino-based RLC component meter	1 Ω – 1 MΩ	1 pF-1000 µF	1µH - 1H	LED display
Panchal et al. (2025), Sensors 25:3688	AD5933 impedance converter + Raspberry Pi 4	Impedance, 10 Hz–100 kHz	NRMSE vs benchtop analyser: 1.41% (magnitude), 3.77% (phase)	10 Hz-100kHz	Software display
Commercial handheld (OpenLCR, 2022)	Calibrated handheld LCR meter	Broad	≈ 0.3%	$300–500	Not stated
Commercial bench (OpenLCR, 2022)	Metrology-grade LCR meter	Broad	Up to 0.02%	$3,000–12,000	Not stated

4. CONCLUSION

A low-cost, microcontroller-based digital RLC meter integrated with an oscilloscope interface for real-time waveform and phase analysis has been designed, fabricated, and evaluated. Operating on an Arduino Pro Mini platform (ATmega328P) with an external 16 MHz crystal oscillator, the system successfully measures resistance via potential division and determines inductance and capacitance through op-amp-based relaxation and LC oscillation techniques. The hardware architecture comprising a regulated 5 V power stage, slave signal-conditioning board, three-way mode selection switch, 2×16-character LCD, and BNC oscilloscope output was successfully assembled on Vero board at a total Bill of Materials (BOM) cost of approximately $16.65 USD. This represents a cost savings of over 44% compared to basic uncalibrated handheld meters and over 94% compared to entry-level commercial handheld LCR meters, while uniquely adding real-time signal visualization.

Through rigorous recalculation and statistical re-evaluation of the experimental measurement data, the instrument's performance relative to nominal component values was established:

- **Resistance Measurement:** Exhibited a Mean Absolute Percentage Error (MAPE) of 3.12% with a maximum deviation of 8.33% (R_1, 1.2 kΩ) Statistical analysis confirmed a significant, near-constant negative bias (mean bias −3.12%, $p = 0.018$) caused by a fixed −0.1 Ω lead/contact resistance offset rather than a scale error. Six out of seven tested resistors fell within their stated ± 5 % tolerance limits.

© 2026 The Authors. Published by Bexford Publishing Ltd

- **Capacitance Measurement:** Achieved a MAPE of 0.62% (maximum error 1.00% at 10 µF) with no statistically significant bias (mean bias +0.17%, p = 0.52), with 8/8 tested components falling within their specified ± 20\% tolerance.
- **Inductance Measurement:** Achieved a MAPE of 1.97% (maximum error 4.88% at 8.2 mH) with no statistically significant bias (mean bias +0.37, p = 0.70), with 8/8 tested components falling within their specified ±10% tolerance.

Oscilloscope observations verified that the resistance measurement loop operates as an RC relaxation oscillator, producing sinusoidal/exponential charging curves whose oscillation frequency is inversely proportional to resistance ($f \alpha Rx^{-1}$), directly explaining the observed log–log regression slope of -0.96 ± 0.23. Inductive components produced characteristic sawtooth waveforms. Time-domain voltage–current traces successfully demonstrated reactive phase behavior, showing current lagging voltage in inductive modes and current leading voltage in capacitive modes. Theoretical uncertainty modeling confirmed that 10-bit ADC quantization, combined with a 100 ms timer gate interval and ± 1% reference components, limits the mid-scale expanded uncertainty (k = 2) to ± 1.2\% for resistance and ± 1.64 for inductance and capacitance, bounding the metrological floor of the current hardware design.

The detailed Bill of Materials (BOM) or the locally developed microcontroller-based digital RLC meter for this study.

Table 11: The Bill of Materials (BOM) for constructing the low-cost microcontroller-based digital RLC meter sums to $16.65 USD.

Item No.	Component Description	Specifications / Model	Quantity	Unit Price (Total Cost (USD))
1	Microcontroller Board	Arduino Pro Mini (ATmega328P, 16 MHz, 5 V)	1	$3.50
2	Display Module	2×16 Character LCD Display	1	$2.00
3	Voltage Regulator	LM7805 (+5 V Linear Voltage Regulator)	1	$0.40

© 2026 The Authors. Published by Bexford Publishing Ltd

4	Operational Amplifiers	Op-Amps (LM358 / TL082 dual op-amp DIP)	2	$0.50
5	Mode Selection Switch	3-Way Selector Switch (Capacitance / Inductance / Resistance)	1	$0.80
6	Push Button	Tactile Push Button (Pulse trigger)	1	$0.15
7	Test Terminal Block	6-Pin PCB Screw Terminal Block	1	$0.60
8	Prototyping Board	Vero Board / Stripboard	2	$1.00
9	Enclosure / Casing	Plastic/Metal Utility Junction Enclosure	1	$3.00
10	Reference Passive Components	Precision Resistors, Reference Inductor, & Capacitors	1 set	$1.20
11	Connectors & Hardware	BNC Connector, Wires, Screws, & Headers	1 set	$2.00
Total				**$16.65 USD**

Key Notes:

© 2026 The Authors. Published by Bexford Publishing Ltd

- **Cost Comparison:** Fabrication at **$16.65 USD** offers over **44% savings** compared to basic uncalibrated handheld meters (~ $30) and over **94% savings** compared to standard commercial handheld LCR meters ($300 – $500).
- **Architecture:** The design pairs an **ATmega328P** with op-amp signal conditioning and a BNC output interface for real-time waveform inspection on an external oscilloscope.

Declarations

Funding: Authors declare no funding for this research

Competing interests: The authors declare that they have no competing interests

Conflicts of interest: The authors declare that they have no conflict of interest

Availability of data: The datasets generated during and/or analyzed during the current study are not publicly available but are available from the corresponding author on reasonable request.

Ethical Approval: Not applicable

Code availability: Not applicable

Acknowledgments

The authors acknowledge the availability of laboratory facilities and components that enabled the construction and testing of the prototype instrument.

References

Agarwal, A., & Lang, J. H. (2005). *Foundations of Analog and Digital Electronic Circuits*. Morgan Kaufmann.

Alexander, C. K., & Sadiku, M. N. O. (2016). *Fundamentals of Electric Circuits* (6th ed.). McGraw-Hill Education.

An7orAhmed. (2025). *Arduino-Based-RLC-Component-Meter* [GitHub repository]. GitHub.

Baccigalupi, A., Daponte, P., & Grimaldi, D. (1994). On a circuit theory approach to evaluate the stray capacitances of two coupled inductors. *IEEE Transactions on Instrumentation and Measurement*, 43(5), 774–776.

Balabanian, N., & Bickart, T. A. (1981). *Electrical Network Theory*. John Wiley & Sons.

Boylestad, R. L. (2015). *Introductory Circuit Analysis* (13th ed.). Pearson.

Casas, O., & Pallas-Areny, R. (1996). Basics of analog signal conditioning for sensors. *IEEE Transactions on Instrumentation and Measurement*, 45(1), 275–279.

Dorf, R. C., & Svoboda, J. A. (2018). *Introduction to Electric Circuits* (9th ed.). John Wiley & Sons.

Floyd, T. L. (2010). *Principles of Electric Circuits: Conventional Current Version* (9th ed.). Pearson.

Franco, S. (2014). *Design with Operational Amplifiers and Analog Integrated Circuits* (4th ed.). McGraw-Hill Education.

Franco, S. (2002). *Electric Circuits Fundamentals*. Oxford University Press.

Haque, B. (1971). *Alternating Current Bridge Methods*. Pitman.

Herres, D. (2020). *Oscilloscopes: A Manual for Students, Engineers, and Scientists* (1st ed.). Springer.

© 2026 The Authors. Published by Bexford Publishing Ltd

Horowitz, P., & Hill, W. (2015). *The Art of Electronics* (3rd ed.). Cambridge University Press.

Hu, C. (2010). *Modern Semiconductor Devices for Integrated Circuits*. Pearson.

Inácio, P. M. C., Guerra, R., & Stallinga, P. (2022). An ultra-low-cost RCL-meter. *Sensors*, 22(6), 2227.

Jaeger, R. C., & Blalock, T. N. (2015). *Microelectronic Circuit Design* (5th ed.). McGraw-Hill Education.

Joint Committee for Guides in Metrology (JCGM). (2008). *Evaluation of Measurement Data — Guide to the Expression of Uncertainty in Measurement (GUM 1995 with minor corrections)* (JCGM 100:2008). BIPM.

Marioli, D., Sardini, E., & Taroni, A. (1993). High accuracy measurement techniques for capacitance transducers. *Measurement Science and Technology*, 4(3), 337–343.

Middlebrook, R. D. (1989). Measurement of loop gain in feedback systems. *International Journal of Electronics*, 38(4), 485–512.

Monk, S. (2016). *Programming Arduino: Getting Started with Sketches* (2nd ed.). McGraw-Hill Education.

Nilsson, J. W., & Riedel, S. (2019). *Electric Circuits* (10th ed.). Pearson.

Nise, N. S. (2019). *Control Systems Engineering* (8th ed.). John Wiley & Sons.

OpenLCR. (2022). *Open-source LCR meter project* [GitHub repository]. GitHub.

Oppenheim, A. V., & Willsky, A. S. (1997). *Signals and Systems* (2nd ed.). Pearson Prentice Hall.

Pallás-Areny, R., & Webster, J. G. (2001). *Sensors and Signal Conditioning* (2nd ed.). John Wiley & Sons.

Panchal, J., Singh, M. I., Singh, M., & Sandha, K. S. (2025). Design and validation of low-cost, portable impedance analyzer system for biopotential electrode evaluation and skin/electrode impedance measurement. *Sensors*, 25(12), 3688.

Proakis, J. G., & Manolakis, D. G. (2006). *Digital Signal Processing: Principles, Algorithms, and Applications* (4th ed.). Pearson.

Qutob, S., Teng, M. F., & Wibawa, A. P. (2024). Specialized capacitor meter for a portable, low-cost electronics education laboratory. *2024 IEEE Global Engineering Education Conference (EDUCON)*, 1–4.

Ramshaw, R., & van Heeswijk, R. (1990). *Energy Conversion: Statics and Dynamics*. Saunders College Publishing.

Reverter, F., & Pallàs-Areny, R. (2005). Direct interface circuit for capacitive sensors. *IEEE Transactions on Instrumentation and Measurement*, 54(4), 1599–1605.

Savant, C. J., Roden, M. S., & Carpenter, G. L. (2002). *Electronic Design: Circuits and Systems* (3rd ed.). Addison-Wesley.

Sedra, A., & Smith, K. (2014). *Microelectronic Circuits* (7th ed.). Oxford University Press.

Smith, S. W. (1997). *The Scientist and Engineer's Guide to Digital Signal Processing*. California Technical Publishing.

Taylor, J. R. (1997). *An Introduction to Error Analysis: The Study of Uncertainties in Physical Measurements* (2nd ed.). University Science Books.

Tocci, R. J., Widmer, N. S., & Moss, G. L. (2017). *Digital Systems: Principles and Applications* (12th ed.). Pearson.

© 2026 The Authors. Published by Bexford Publishing Ltd

Tumanski, S. (2006). *Principles of Electrical Measurement*. CRC Press.

Van Valkenburg, M. E. (1974). *Network Analysis* (3rd ed.). Prentice-Hall.

Webster, J. G., & Eren, H. (Eds.). (2014). *Measurement, Instrumentation, and Sensors Handbook* (2nd ed.). CRC Press.

Williams, A. B., & Taylor, F. J. (2006). *Electronic Filter Design Handbook* (4th ed.). McGraw-Hill Education.

Xie, Y. M., Wan, G. C., & Tong, M. S. (2023). A novel LCR impedance detection system with low cost and high precision based on microcontroller unit. *2023 Photonics & Electromagnetics Research Symposium (PIERS)*, 1840–1845.

Ziemer, R. E., Tranter, W. H., & Fannin, D. R. (2014). *Signals and Systems: Continuous and Discrete* (4th ed.). Pearson.

© 2026 by the authors. Submitted for possible open access publication under the terms and conditions of the **Creative Commons Attribution (CC BY 4.0) licence** (https://creativecommons.org/licenses/by/4.0/)